THE JOURNAL OF PHYSICAL CHEMISTRY B
A JOURNAL OF THE AMERICAN CHEMICAL SOCIETY

pubs.acs.org/JPCB

Article

Transient Electrostatic Interactions between Fcp1 and Rap74 Bias the Conformational Ensemble of the Complex with Minimal Impact on Binding Affinity

Victor A. Prieto, Kevin E. W. Namitz, and Scott A. Showalter*

Cite This: J. Phys. Chem. B 2021, 125, 10917−10927

Read Online

ACCESS | Metrics & More | Article Recommendations | Supporting Information

ABSTRACT: Intrinsically disordered protein (IDP) sequences often contain a high proportion of charged residues in conjunction with their high degree of hydrophilicity and solvation. For high net charge IDPs, long-range electrostatic interactions are thought to play a role in modulating the strength or kinetics of protein−protein interactions. In this work, we examined intramolecular interactions mediated by charged regions of a model IDP, the C-terminal tail of the phosphatase Fcp1. Specifically, this work focuses on intermolecular interactions between acidic and basic patches in the primary structure of Fcp1 and their contributions to binding its predominantly basic partner, the winged helix domain of Rap74. We observe both intramolecular and intermolecular interactions through paramagnetic relaxation enhancement (PRE) consistent with oppositely charged regions associating with one another, both in unbound Fcp1 and in the Fcp1−Rap74 complex. Formation of this complex is strongly driven by hydrophobic interactions in the minimal binding motif. Here, we test the hypothesis that charged residues in Fcp1 that flank the binding helix also contribute to the strength of binding. Charge inversion mutations in Fcp1 generally support this hypothesis, while PRE data suggest substitution of observed transient interactions in the unbound ensemble for similarly transient interactions with Rap74 in the complex.

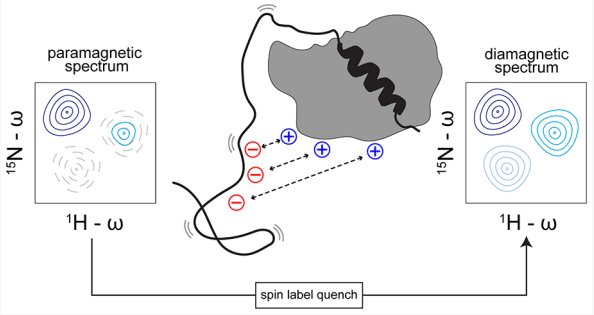

INTRODUCTION

Intrinsically disordered proteins (IDPs), which favor a diverse ensemble of conformations that exchange over time, as opposed to adoption of persistent and unique secondary or tertiary structure, are widespread in eukaryotic proteomes, suggesting their importance in a diverse set of biological processes.[1,2] Early studies of transcriptional activation domains revealed striking examples of the importance of charge in IDP function, as best exemplified by the acidic transactivation domains that feature disordered structure and an abundance of negative charge.[3] Acidic domains of IDPs have also been linked to macromolecular assembly, such as in the recruitment of Rpn3 and Rpn7 into the proteasome lid complex by the disordered protein Sem1.[4] Subsequent bioinformatic studies confirmed the enrichment of charged residues in IDP sequences and a lack of the bulky, hydrophobic residues that drive other proteins to fold.[5,6] Instead, IDPs interconvert between many solvent-exposed conformations in their solution ensemble due to their comparatively high hydrophilicity and freedom from having to desolvate a hydrophobic surface as a driver of folding. The functions of numerous IDPs are tied to biases in their conformational ensembles, which are under the control of factors like proline content, ligand binding, and charge distribution among side-chains.[7−9] Charge enrichment may also impart hitherto underinvestigated functions that impact the stability of binding complexes or the kinetics of interactions with IDP binding partners.

To explore how clusters of amino acids imparting high net charge impact the conformational ensemble biases and intermolecular interactions of a well-studied IDP, we have chosen the C-terminal domain of the transcription factor II-F (TFIIF) associating RNA polymerase II (RNA Pol II) C-terminal domain phosphatase 1, known generally as Fcp1. The C-terminal domain of Fcp1 drives its recruitment to RNA Pol II through interaction with a winged-helix domain found in the Rap74 subunit of TFIIF (Figure 1A).[10] Recruitment of Fcp1 is necessary during a step of the RNA Pol II C-terminal domain (CTD) phosphorylation/dephosphorylation cycle that is associated with termination of mRNA synthesis and subsequent polymerase recycling.[11] Two disordered domains of Fcp1 bind to Rap74: a central domain and the aforementioned C-terminal region that will be termed "ctFcp1" throughout.[12] The properties of ctFcp1 have been rigorously explored in

Received: June 10, 2021
Revised: September 7, 2021
Published: September 22, 2021

https://doi.org/10.1021/acs.jpcb.1c05131
J. Phys. Chem. B 2021, 125, 10917−10927

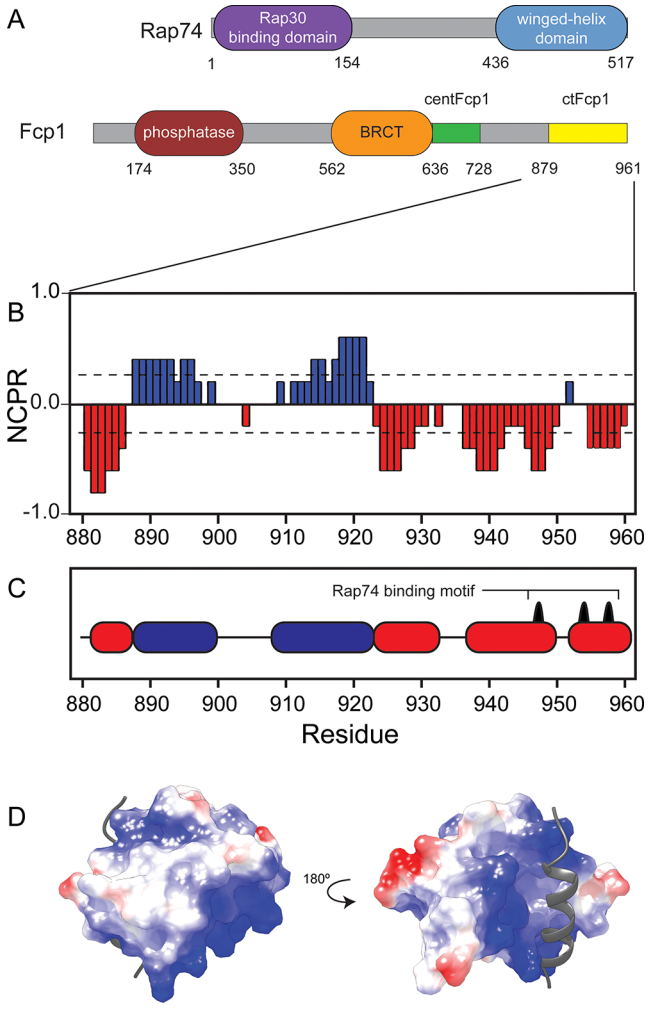

Figure 1. Interacting regions of Rap74 and Fcp1 are highly charged. (A) Domain architecture and human amino acid sequence numbering for Rap74 and Fcp1. Folded protein domains are represented as wide rounded rectangles, while disordered regions are narrow, sharp-cornered rectangles. (B) Net charge per residue, generated by CIDER,[37] for the C-terminal Rap74-interacting region of Fcp1 (ctFcp1, residues 879–961). The net charge for a residue is calculating with a blob containing five residues centered on the residue in question and plotted against residue number. (C) Cartoon representation of ctFcp1's charge distribution used throughout this article to aid in data interpretation. The color scheme is the same used above, while the three hydrophobic residues in the interaction domain known to make essential contacts with Rap74 are indicated by black rounded cones protruding from the C-terminal region. (D) Distribution of charges on the Rap74 winged-helix domain surface (PDB ID 1j2x). The ctFcp1 ribbon (gray) indicates the location of the binding cleft. Red, blue, and white colored on Rap74 indicate acidic, basic, and neutral electrostatic surface, respectively; coloration was generated by using the Coulombic surface coloring tool packaged in Chimera.

studies from our lab, especially in the context of its helical propensity and the thermodynamic properties of its binding interaction.[13−15] ctFcp1 is mostly disordered except for a region between residues 944 and 961, which is found within the 16 residues of ctFcp1 that form an α-helix in the Fcp1/Rap74 complex and that also samples an α-helix in the unbound state. Preformed helicity in disordered proteins has been shown to have a complex impact on both association rate and complex stability for binding to folded proteins.[16,17] The stabilization of the α-helix structure in Fcp1 is concomitant with binding to a hydrophobic cleft in the winged-helix domain of Rap74. X-ray crystallographic and NMR studies show that ctFcp1 is anchored to Rap74 by three hydrophobic side-chains and two salt bridges that flank the helix.[18,19] In the NMR study, which unlike the crystallographic structure included residues 879–940 of ctFcp1, nuclear Overhauser enhancements (NOEs) were not observed between Rap74 and the aforementioned N-terminal residues of ctFcp1. The lack of NOEs for this region of ctFcp1 is consistent with the nonhelical segment of ctFcp1 remaining largely dynamic in this "fuzzy" complex.[20−22]

It is perhaps surprising that only two intermolecular salt bridges are observed in the solved structure of the complex, given the high prevalence of basic amino acids on the surface of Rap74 and the high fraction of charged resides and net negative charge of Fcp1 adjacent to the minimal binding motif. The positive charge on Rap74 is concentrated in two locations: surrounding the binding cleft and on the face directly opposite the binding cleft. Like many IDPs, ctFcp1 displays polyampholytic character: the 15 residues adjacent to the binding helix are highly acidic, while the next 30 residues feature two patches of net positive charge with acidic residues interspersed (Figure 1B,C).[23] A strong representation of charged residues within the ctFcp1/Rap74 system suggests that electrostatic interactions beyond the core binding helix contribute to the stability of the complex, despite the highly dynamic character of the Fcp1 charged region in the complex.

In this study we tested the hypothesis that charge complementarity between Rap74 and charged patches in ctFcp1 that flank the binding helix lead to net stabilization of the complex. To perform this work, we leveraged the ability of solution NMR to characterize IDP structure and function through characterization of unbound IDP conformation and also the conformational biases of IDP regions that remain dynamic in complexes.[24] Paramagnetic relaxation enhancement (PRE) NMR techniques have been successfully used to explore IDP structure,[25−27] as demonstrated through our prior investigation of the ensemble behavior of a disordered region from the transcription factor Pdx1.[28] Therefore, we used PRE to identify biases in the unbound ctFcp1 conformational ensemble and to investigate electrostatic contributions to the interaction between ctFcp1 and Rap74. Our data show that regions of opposite charge within ctFcp1 do transiently associate in the unbound state and make subtle contributions to association with Rap74. In addition, when mutants designed to invert the local charge in key regions of ctFcp1 were tested, we observed a shift in the interactions that maintain associations between regions of opposite charge and retention of the overall dynamic character of the helix-flanking region of ctFcp1.

METHODS

Construct Preparation. The coding sequences for residues 879–961 of human Fcp1 (ctFcp1) or residues 435–520 of human Rap74 were cloned into pET47b as described previously, such that the resulting proteins contain an N-terminal 6xHis tag and HRV 3CProtease recognition site in frame.[13] As both ctFcp1 and Rap74 lack endogenous cysteine residues needed for PRE studies (see below), Quikchange (Agilent) or Q5 site-directed mutagenesis (NEB) kits were used to generate single replacement of residues in ctFcp1 and Rap74 with cysteines at the following sites: Gly892, Ala927,

https://doi.org/10.1021/acs.jpcb.1c05131
J. Phys. Chem. B 2021, 125, 10917−10927

Ala935, and Met961 in ctFcp1 and Ser485 in Rap74. To facilitate quantification of Rap74 concentration by UV−vis spectroscopy, a codon was inserted into the Rap74 plasmid encoding an exogenous tryptophan at the N-terminus, following the 3C-Protease cleavage site, resulting in an N-terminal Gly-Pro-Gly-Trp cloning artifact in the final construct.

Q5 mutagenesis was employed to replace charged residues in ctFcp1 with oppositely charged counterparts, creating charge variants. An exogenous cysteine was retained in all charge variants at residue 927 for spin-label conjugation. A full list of charge variants and charge-flip mutations can be found in Table 1. Successful mutagenesis was confirmed by Sanger sequencing at the Huck Institutes Genomic Core Facility at Penn State.

Table 1. ctFcp1 Charge Variant Constructs

ctFcp1 construct	net charge[a]	mutations
EDE	−14.02	K919E, R920D, K921E
wild type	−8.00	
3K	−1.98	E924K, E925K, E930K
KRK	−1.98	E938K, D939R, E940K
5KR	+4.04	E924K, E925K, E930K, E938K, D939R, E940K

[a]Net charge calculated by using CIDER.[37]

Protein Expression and Purification. BL21(DE3)-FhuA2$^-$ cells containing the Rap74 plasmid were grown in Terrific Broth media in a Sartorius Biostat B-DCU 5 L vessel until the culture reached an optical density at 600 nm (OD_{600}) of 0.7. Expression was induced by the addition of 0.5 mM IPTG, and the cells were harvested after a 29 h incubation at 18 °C. Other recombinant proteins were grown in shaker flasks and expressed at 37 °C for 3−4 h. ^{13}C and ^{15}N isotopic enrichment for NMR samples was achieved by growing in M9 minimal media supplemented with ^{13}C-glucose and ^{15}N-ammonium chloride, respectively. Protein expression was induced with 0.5 mM IPTG when OD_{600} reached between 0.6 and 0.7. Proteins not requiring isotopic enrichment were expressed in cells grown in Luria broth and induced identically, but in an OD_{600} range of 0.7 and 0.9. Cells were pelleted by centrifugation, washed in 20 mM tris(hydroxymethyl)-aminomethane, 20 mM sodium chloride, and 1 mM ethylenediaminetetraacetic acid, pH 7.5, and frozen at −80 °C for later purification. Cells were lysed by sonication in lysis buffer (50 mM Tris, pH 7.5, 500 mM NaCl, and 20 mM imidazole) supplemented with 5 mM 2-mercaptoethanol, 1 mM PMSF, and 1X commercial protease inhibitor (Millipore). Lysate clarified by centrifugation at 14000*g* was passed through a 5.0 μm filter and then run over a Ni-NTA column. The column was washed in lysis buffer plus 0.1% Triton X-100 prior to eluting in lysis buffer supplemented with 200 mM imidazole. The elution fraction was treated with HRV 3C protease and dialyzed overnight at 4 °C against 50 mM Tris, pH 7.5, 500 mM NaCl, and 5 mM 2-mercaptoethanol. The dialyzed material was then run again over a Ni-NTA column to isolate the protein of interest in the flowthrough. Proteins intended for PRE experiments were purified similarly, except imidazole was removed via serial dilution with imidazole-free lysis buffer and reconcentration in Amicon Ultra Centrifugal Filters. Protein purity was assessed by SDS-PAGE. Proteins for fluorescence anisotropy experiments were further purified by size exclusion chromatography over a Sephadex G-100 column in SEC buffer (50 mM Tris, pH 7.5, 500 mM NaCl, 5 mM dithiothreitol). Purified proteins were buffer exchanged into 20 mM sodium phosphate and 100 mM sodium chloride, pH 7.0 for all experiments. For plate-based binding assays, a 10% (w/v) stock solution of BSA was added to 1% to inhibit protein adhesion to the well walls. The protein concentration was determined by FTIR (MilliporeSigma) or by A_{280}.

Spin-Labeling Cysteine Mutants. All cysteine mutants were allowed to incubate with 10 mM DTT (at least 5-fold molar excess) for a minimum of 30 min at 4 °C. DTT was removed by using a desalting PD-10 column. The eluted protein was treated with 5 mol equiv of the paramagnetic spin-label MTSL (*S*-(1-oxyl-2,2,5,5-tetramethyl-2,5-dihydro-1*H*-pyrrol-3-yl)methylmethanesulfonothioate). The conjugation reaction was completed by incubating for 30 min at 4 °C in the dark, and then excess MTSL was removed by the same desalting column. No reducing agents were brought into contact with samples from this point forward to avoid cleaving MTSL from cysteines. MTSL conjugation was confirmed by mass spectrometry. Proteins that were not labeled with MTSL were passed over the PD-10 column once to exchange into the same buffer system. The final buffer conditions for PRE samples were 20 mM sodium phosphate, 100 mM sodium chloride, pH 7.0, 1% (v/v) D_2O, 1 mM PMSF, 1 mM EDTA, 1X Calbiochem Protease Inhibitor Cocktail Set V, and 0.01% (v/v) NaN_3.

Paramagnetic Relaxation Enhancement (PRE) Experiments. PRE experiments were conducted at 298 K on Bruker Avance NEO or Avance III spectrometers, both operating at 600 MHz (14.1 T) and equipped with TCI cryoprobes. Chemical shift assignments for *apo*-ctFcp1 Rap74 have been previously reported.[13,19] Residues adjacent to the incorporated cysteines were either assigned by triple resonance experiments or deduced from residue position and PRE intensity. Intramolecular PRE experiments conducted on spin-labeled, $^{13}C-^{15}N$-enriched ctFcp1 cysteine mutants were recorded by the (HACA)-CON experiment using 32 scans with 1024 and 256 points in the direct (^{13}C) and indirect (^{15}N) dimensions, respectively. Intermolecular PRE experiments conducted on ^{15}N-enriched Rap74, and spin-labeled ctFcp1 cysteine mutants were recorded by standard $^1H,^{15}N$-HSQC, using 32 scans with 2048 and 256 points in the direct (^1H) and indirect (^{15}N) dimensions, respectively. The control intramolecular PRE experiment in which ^{15}N-enriched Rap74 was spin-labeled at Cys485 was collected with identical NMR parameters. All intermolecular PRE experiments were performed with a 2:1 molar excess of spin-labeled, natural isotope abundance ctFcp1 to ^{15}N-Rap74. To complete the diamagnetic control experiments, the paramagnetic spin-label was quenched by directly adding 1 μL of 0.5 M sodium ascorbate in 0.2 M sodium phosphate, pH 7.0, to the NMR tube.

Fluorescence Anisotropy Binding Assays. A synthetic peptide of residues 940−961 of Fcp1 with an N-terminal FITC-Ahx fluorescent tag was purchased from GenScript, dissolved in phosphate buffered saline, and stored in 1 mM aliquots at −80 °C. This construct, which we termed f-Fcp1x, was designed to contain the same Fcp1 residues as the crystallographic construct used by Kamada et al. in 2003.[18] For direct measurements of the binding constant of f-FCP1x, Rap74 was varied against f-FCP1x held constant at 40 nM. Samples were incubated at room temperature in darkness for 30 min to ensure complete equilibration before loading wells.

https://doi.org/10.1021/acs.jpcb.1c05131
J. Phys. Chem. B 2021, 125, 10917−10927

Each titration was performed with three technical replicates, and each well contained 30 μL of sample. Fluorescence anisotropy competitive binding assays were set up similarly to the direct titration, but with the f-Fcp1x and Rap74 concentrations held constant in each well at 40 nM and 10 μM, respectively, while the concentration of competitor Fcp1 construct was varied across the titration. In all experiments, fluorescence anisotropy was measured at 24 °C on a Tecan Infinite M1000 Pro. The fluorescent tag was excited at 470 nm, and parallel and perpendicular intensities were collected at 516 nm over 400 ms. Data were fitted by using an in-house Python script, where the fitting function was defined by using the framework described by Roehrl et al.[29]

Circular Dichroism. CD was used to monitor changes in secondary structure associated with the charge variation mutations in ctFcp1. All CD data were collected on a Jasco J-810 spectrophotometer purged with N_2. Each protein was 0.1−0.2 mg/mL in 20 mM potassium phosphate, pH 7.0. The A927C mutant had 500 μM 2-mercaptoethanol added to this buffer to keep the cysteine residue reduced. A 0.1 mm quartz cuvette was used. Measurements were taken from 205 to 260 nm at 20 °C with data points recorded every 1 nm and a bandwidth of 2 nm. Three separate scans were averaged for each experiment.

Simulated PRE Data. A pool of 1×10^6 ctFcp1 conformers, used to determine interresidue distances (α carbons) for simulated PRE values of proteins exhibiting perfectly random coil behavior, was produced by using RANCH from the ATSAS EOM 2.0 package.[30,31] Simulated PRE ratios for each resonance were generated by using the following equation adapted from Battiste and Wagner:[32]

$$\frac{I_{ox}}{I_{red}} = \frac{R2\ \exp(-R2^{sp}t)}{R2 + R2^{sp}} \quad (1)$$

where $R2$ and $R2^{sp}$ are the intrinsic spin relaxation rate of ^{13}C and the rate of spin relaxation contributed by the paramagnetic center, respectively, and t is the total evolution time of the transverse magnetization during the experiment (12.5 ms). For our calculations of ^{13}C relaxation, $R2$ was set to 8.1 s^{-1}. $R2^{sp}$ itself is related to the distance between the paramagnetic center and the atom carrying transverse magnetization by the equation

$$r = \left[\frac{K}{R_2^{sp}}\left(4\tau_c + \frac{3\tau_c}{1 + \omega^2\tau_c^2}\right)\right]^{1/6} \quad (2)$$

where ω is the Larmor frequency for ^{13}C ($\omega_{^{13}C} = 2\pi \times 600 \times 10^6\ s^{-1}$) and τ_c is ctFcp1's estimated rotational correlation time (20.7 ns). The parameter K is composed of fundamental constants:

$$K = \frac{1}{15}S(S+1)\gamma^2 g^2 \beta^2 \quad (3)$$

where S and γ are the spin quantum number and gyromagnetic ratio for the excitation nucleus, g is the electron g-factor, and β is the Bohr magneton. For ^{13}C, K is equal to about $7.778 \times 10^{-34}\ cm^6\ s^{-2}$.

All molecular graphics images were generated by using UCSF Chimera.[33] All other analyses were performed by using in-house Python scripts, with graphs generated in the Matplotlib library (https://matplotlib.org) prior to export into Adobe Illustrator.

RESULTS

This study was motivated by the desire to investigate transient electrostatic interactions in a highly dynamic complex involving an IDP and its folded partner. We have previously demonstrated through NMR spin relaxation that the charged region of ctFcp1 flanking the binding helix remains dynamic in complex with Rap74.[15] Examination of the charge distribution along the polypeptide chain of ctFcp1 spanning residues 879−961 reveals that this well-studied system is an ideal candidate, as visualized in the net charge per residue plot shown in Figure 1B. Both the helical binding region (940−960) and the adjacent 16 residues are acidic. In contrast, from residues 889−923, there is a pronounced enrichment in the basic amino acids lysine and arginine. Even in this region, there are several acidic residues interspersed, underscoring the highly charged nature of the helix-flanking region of ctFcp1.

From the presence of these charged tracts, we posited the existence of long-range contacts in the conformational ensemble of unbound ctFcp1, caused by attraction between regions of opposite charge. Self-association between binding regions and adjacent sequences has been shown to weakly block binding motifs in IDPs, preventing nonspecific binding from occupying the binding site.[34−36] We reasoned from the blocks of opposite charge found in ctFcp1 that such a mechanism may prevent nonspecific adhesion of the amphipathic Rap74-binding helix to off-targets. To identify the presence of this mechanism, we needed to employ a technique to reveal electrostatically mediated contacts, which have a long-range distance sensitivity compared to hydrophobic interactions.

Intramolecular PRE to Probe the Solution Ensemble of Unbound ctFcp1. We sought to map out any transient interactions that might exist within ctFcp1's unbound conformational ensemble using paramagnetic relaxation enhancement (PRE). To produce the paramagnetic protein needed for PRE measurements, a paramagnetic MTSL spin-label was conjugated to ctFcp1 at a single cysteine residue via a disulfide bond. Conveniently, ctFcp1 has no native cysteines, which facilitated specific installation of single cysteines at desired locations throughout the length of the protein. In the PRE experiment, the proximity of a given amino acid residue to the spin-label, either due to being close in the primary structure to the site of cysteine-attachment or due to long-range contacts in the ensemble, results in significant line broadening of associated NMR resonances. Thus, calculating the ratio of per-residue resonance intensity in the sample before and after quenching the paramagnetic radical (producing a diamagnetic state, but otherwise leaving the nitroxide probe intact) yields information about each residue's proximity to the spin-label.

The PRE ratios for *apo*-ctFcp1 with the spin-labels at two different locations, residues 927 and 961, are depicted in Figure 2 (spectra shown in Figure S1, PRE ratios listed in Table S1). In the immediate vicinity of the spin-label, a "well" forms due to intensity ratios decreasing as the residue approaches the cysteine in the protein sequence. The solid black line is a computed prediction of intensity ratios assuming the disordered protein follows perfect random coil behavior, as generated by the ATSAS EOM package (see the Methods section). In ctFcp1, we observed significant resonance intensity loss in the paramagnetic state for several regions distant from the site of spin-label attachment, suggesting that the solution

https://doi.org/10.1021/acs.jpcb.1c05131
J. Phys. Chem. B 2021, 125, 10917−10927

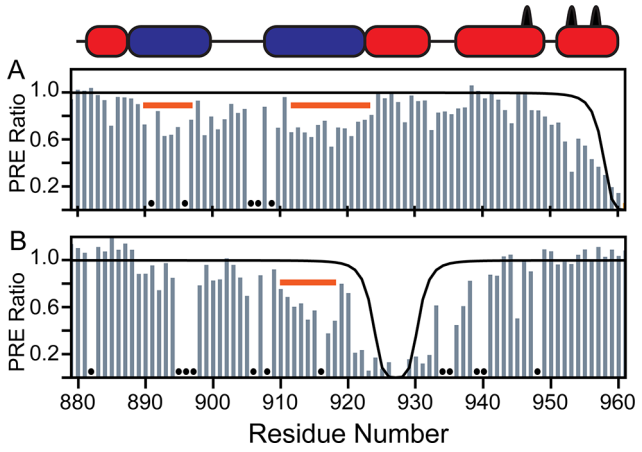

Figure 2. Intramolecular paramagnetic resonance enhancement for ctFcp1 demonstrates a nonrandom structure in solution. The cartoon representation of charge distribution within ctFcp1 is reproduced above to facilitate comparisons between the charge distribution and PRE profile. The paramagnetic spin-label is attached at positions (A) 961 and (B) 927. The solid black line on both plots is a prediction of PRE for a perfect random coil using eqs 1 and 2 to calculate PRE based on distances produced by RANCH from the ATSAS EOM 2.0 package. Horizontal orange bars draw attention to regions of interest with PRE ratios that are unexpectedly low compared to the random coil prediction. Black circles indicate residues removed from the data set due to resonance overlap.

ensemble of ctFcp1 deviates from that of a random coil (Figure 2). With the spin-label at residue 961 (Figure 2A), we observed increased PRE in two regions, both corresponding to the portion of the sequence with net positive charge. We concluded that an association exists between the acidic C-terminal region of ctFcp1 and the basic regions of ctFcp1, although the modest resonance intensity loss suggests this interaction is transient and weak. Attaching the spin-label at residue 927 (Figure 2B) depresses PRE intensity ratios in a region that also corresponds with a region of high positive charge. This PRE intensity pattern persists for both constructs after reducing the ctFcp1 concentration by a factor of 3, suggesting the interaction is intramolecular and not intermolecular in nature (Figure S2). Taken together, these data suggest an intramolecular association between the positively charged region centered on residue 918 and the negatively charged region centered on residue 938, creating a deviation from random coil behavior in the conformational ensemble.

Intramolecular PRE to Probe Changes in the Solution Ensemble of ctFcp1 Introduced by Charge Variants. To test the hypothesis that the interactions observed by PRE in unbound ctFcp1 are driven by electrostatic complementarity in ctFcp1, we generated a series of four mutations designed to reverse the charge of amino acid clusters, retaining the cysteine at position 927 for spin-labeling ctFcp1. We chose to conjugate the spin-label to residue 927 for the charge variants because this site is adjacent to many of the regions of interest identified for wild-type ctFcp1 (Figure 2, orange bars) and so should provide maximum sensitivity as a reporter of charge-sensitive change. In summary, the four clusters of charge inversions introduced were K919E, R920D, K921E (termed EDE throughout); E924K, E925K, E930K (3K); E938K, D939R, E940K (KRK); and E924K, E925K, E930K, E938K, D939R, E940K (5KR). In constructing these charge variants, acidic residues were replaced with lysine residues, with the exception of D939, which was replaced with an arginine to improve spectral characteristics. When generating the EDE mutant to enhance the negative charge of ctFcp1, we preserved the Glu-Lys and Asp-Arg pairing created by the choices made in the positive charge variants. Circular dichroism spectra were collected to confirm that the mutations introduced did not alter the secondary structure of ctFcp1 (Figure S3). Along with wild-type ctFcp1, these constructs span a wide range of net charge per-residue values, as summarized in Table 1.

As expected, the intramolecular PRE profiles for each of the charge-altered constructs varied substantially from that of wild-type (Figure 3; spectra in Figure S4; raw data in Table S1).

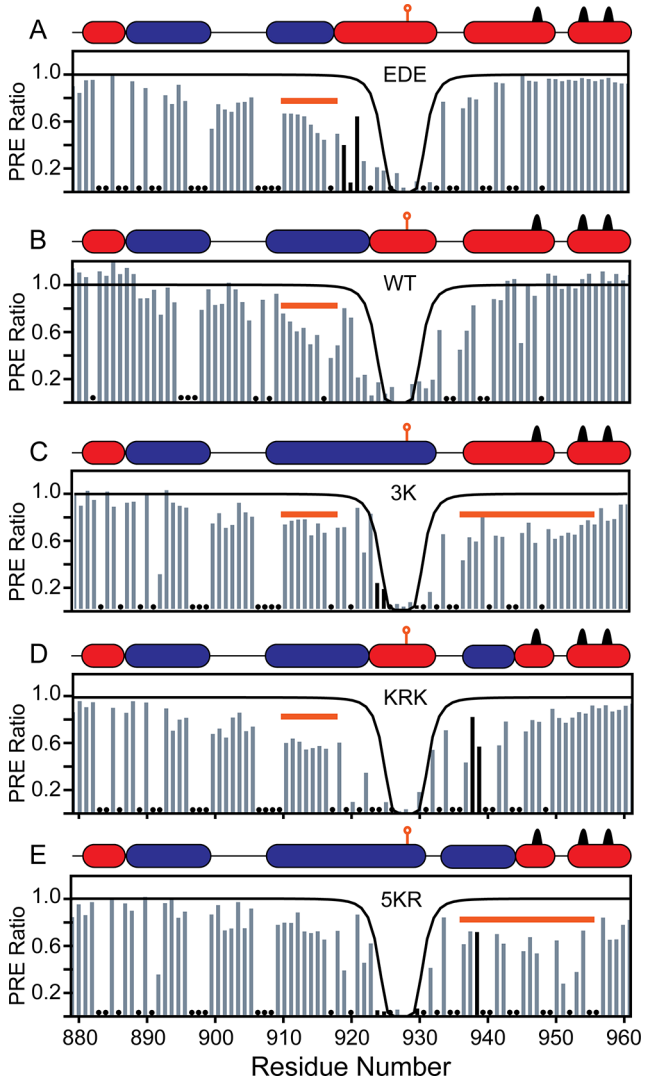

Figure 3. Intramolecular PRE ratios vs residue number for charge-flipped constructs of ctFcp1. All constructs are spin-labeled at residue 927 and named for the residues mutated to flip the local charge density: (A) EDE, (B) wild type, (C) 3K, (D) KRK, and (E) 5KR. Cartoon representations of charge patterning throughout the ctFcp1 charge variants are shown above the corresponding PRE profile. The solid black line is a prediction of PRE for a perfect random chain using eqs 1 and 2 to calculate PRE based on distances produced by RANCH from the ATSAS EOM 2.0 package. Horizontal orange bars draw attention to regions of interest with PRE ratios that are unexpectedly low compared to the random coil prediction. Black circles indicate residues removed from the data set due to resonance overlap.

https://doi.org/10.1021/acs.jpcb.1c05131
J. Phys. Chem. B 2021, 125, 10917−10927

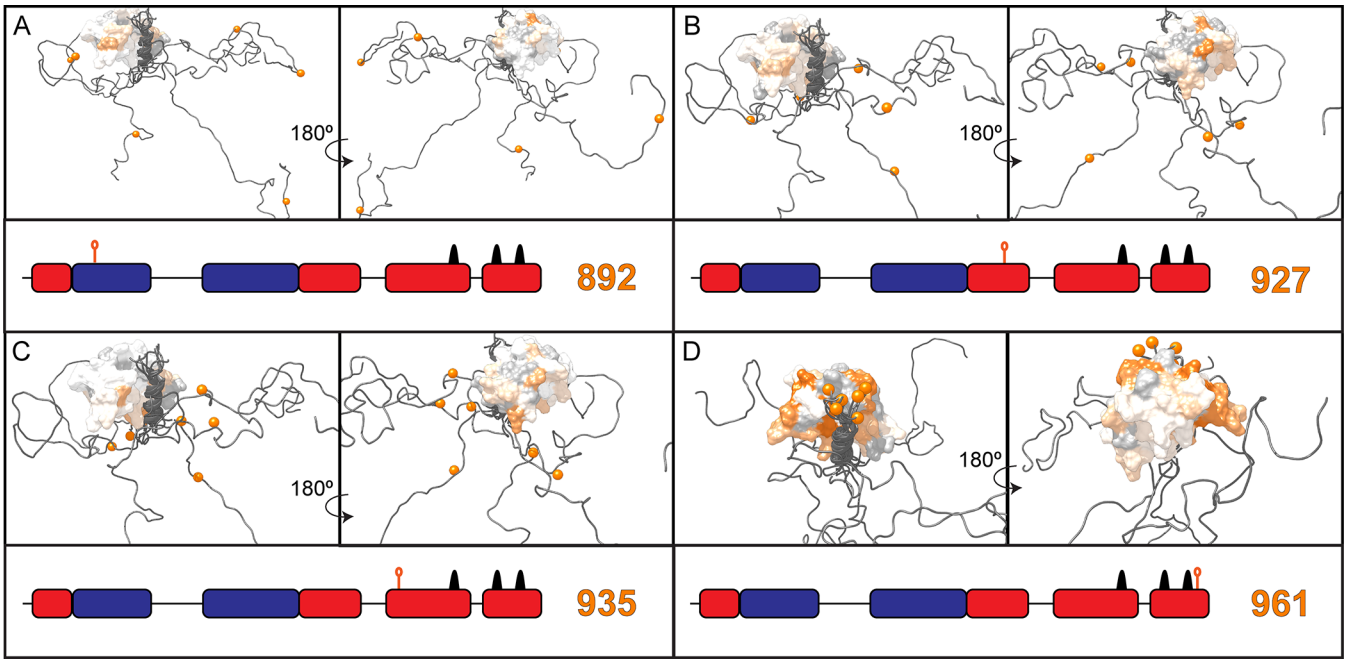

Figure 4. Visualization of PRE on the Rap74 surface with varying spin-label locations. To capture the diversity of ctFcp1 conformations in the complex, five representative ctFcp1 ribbons produced via CAMPARI simulations are overlaid through superposition of residues 940−960. Both sides of the protein complex are shown through rotation by 180°. Cartoon representations of the spin-labeled residue and the charge distribution within ctFcp1 are shown below each pair of PRE figures. The paramagnetic spin-label was attached to four sites within ctFcp1: (A) residue 892, (B) residue 927, (C) residue 935, and (D) residue 961. For each of the five ctFcp1 models shown, the spin-label attachment site is indicated with an orange sphere. PRE intensity is indicated via an orange/white scale, with orange indicating strong signal losses from PRE and white indicating no PRE detected. Rap74 surface shaded gray indicates residues excluded from data set due to resonance overlap or missing resonances.

Compared to the wild-type sequence, the EDE construct shows a greater degree of intensity loss to the N-terminal side with respect to the cysteine residue, while PRE toward the C-terminus remains relatively unchanged. This is consistent with preservation of charge-mediated interactions between the basic regions of ctFcp1 and the region of enhanced negative charge at the site of the EDE mutation. Conversely, the 3K construct, in which positively charged side-chains surround the spin-label, displayed considerably more intensity loss than wild type in the acidic C-terminal region. Unexpectedly, the basic tracts toward the N-terminus also exhibit a deviation from random coil behavior bringing them into proximity with the spin-label at position 927, suggesting significant chain collapse overall in comparison to wild type. This trend continues for the KRK construct, where substantial intensity reduction in the paramagnetic state is observed throughout the chain. In 5KR, where the spin-label is embedded in the longest positively charged region of all the constructs, the C-terminal helix becomes the remaining region with the greatest net-negative charge; here, the PRE profile is similar to that of 3K. However, the spectrum for this construct was compromised through significant resonance overlap, which hindered a more systematic interpretation of the data.

In summary, charge mutations within ctFcp1 produce PRE profiles that differ from wild type in a manner that is consistent with biases in its conformational ensemble that are driven by local electrostatic complementarity. Self-associating interactions in ctFcp1 between the negatively charged binding region and positively charged N-terminal region could lead to several consequences for Rap74 binding. As reviewed above, self-association of the binding helix with the adjacent disordered region could facilitate Rap74 binding by inhibiting nonspecific interactions, which would not provide sufficient Gibbs free energy to overcome the cost of breaking up the intramolecular association. For specific partners, such as Rap74, the binding free energy would be more than sufficient to overcome the weak intramolecular association, although at a cost of somewhat weakened overall affinity compared to that which is anticipated for interaction with the binding helix alone.

Intermolecular PRE to Assess Proximity of ctFcp1 to Charged Regions of the Rap74 Surface. In the previous section, we identified an intramolecular association between the strongly basic N-terminal region of ctFcp1 and the acidic region encompassing the binding helix. Intriguingly, the surface of the Rap74 winged-helix domain has a high net-positive charge adjacent to the Fcp1 binding cleft (Figure 1D). Additionally, we noted a considerable number of positively charged residues on the reverse side of Rap74, facing away from the Fcp1 binding cleft. On the basis of this observation, we hypothesized an interaction between negative patches on Fcp1 and the positive surface of Rap74 exist in the complex, making a favorable contribution to the overall binding free energy.

To test this hypothesis, we again turned to PRE. Instead of intramolecular PRE with the spin-label attached to the isotopically enriched protein detected in the NMR experiment, we observed intermolecular PRE on a sample of isotopically enriched Rap74, while keeping the spin-label attached to ctFcp1. We installed the spin-label in four locations along ctFcp1: residues 892, 927, 935, or 961 (Figure 4; spectra in Figure S5; raw data in Table S2). Mapping the loss of resonance intensity due to PRE on the surface of Rap74 indicates areas where the disordered tail of ctFcp1 approached Rap74 (shaded orange in Figure 5). Attachment of MTSL to

https://doi.org/10.1021/acs.jpcb.1c05131
J. Phys. Chem. B 2021, 125, 10917−10927

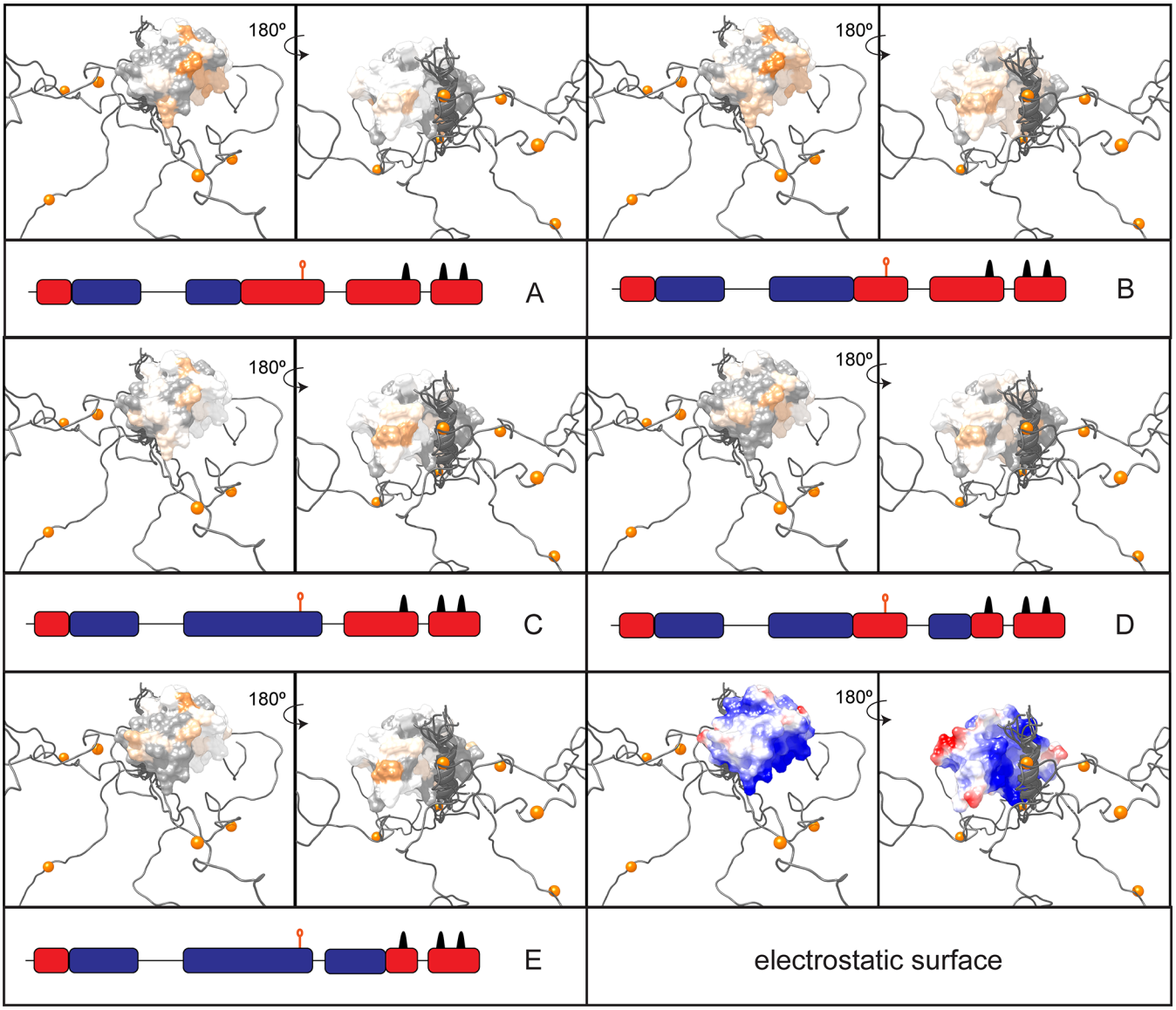

Figure 5. Visualization on the Rap74 surface of PRE from spin-labeled ctFcp1 charge variants. To capture the diversity of ctFcp1 conformations in the complex, five representative ctFcp1 ribbons produced via CAMPARI simulations are overlaid through superposition of residues 940−960. Both sides of the protein complex are shown through rotation by 180°. For each of the five ctFcp1 models shown, the spin-label attachment site is indicated with an orange sphere. Charge variants are (A) EDE, (B) wild type, (C) KRK, (D) 3K, and (E) 5KR. Representative cartoons delineate the charge distribution within ctFcp1 beneath each pair of PRE figures. The paramagnetic spin-label (orange sphere) is attached to residue 927 in each panel. PRE intensity is indicated via an orange/white scale, with orange indicating strong signal losses from PRE and white indicating no PRE detected. Rap74 surface shaded gray indicates residues excluded from data set due to resonance overlap or missing resonances. The electrostatic surface is colored red, blue, and white for acidic, basic, and neutral side-chains, respectively, by using the Coulombic surface coloring tool packaged in Chimera.

residue 961, which is immediately adjacent to the binding helix, resulted in nearly complete resonance loss from Rap74 residues associated with the binding cleft. As a positive control, direct attachment of MTSL to Rap74 after mutating Ser485 to Cys produced a similarly intense resonance loss (Figure S6). In contrast, we observed minimal PRE in Rap74 with the spin-label at residue 892 of ctFcp1, which is expected given the significant distance in primary structure between this attachment site and the binding helix. As a negative control, we repeated the experiment with MTSL attached to Pdx1, a different IDP studied in our lab that shows no affinity for Rap74, resulting in no PRE observed on Rap74 (Figure S1B), thus confirming our interpretation of the Cys892 result.

When PRE was recorded with spin-labels at residue 927 or 935, intermediate levels of resonance intensity loss were observed throughout Rap74, suggesting that the N-terminal disordered region of ctFcp1 does sample conformations in which it is close to the surface of Rap74. Intriguingly, with the spin-label at residue 927 (within the acidic region), we noticed increased PRE on the basic surface of Rap74 compared to the neutral face, while the comparatively small regions of the Rap74 surface with negative charge lacked any intensity loss. This further suggests the charge of the side-chains surrounding the spin-label on ctFcp1 plays an important role in stabilizing association between the two proteins. To test whether the proximity of ctFcp1 in the region of residues ∼920−940 is simply driven by steric effects (residues close to the binding

https://doi.org/10.1021/acs.jpcb.1c05131
J. Phys. Chem. B 2021, 125, 10917−10927

helix will by necessity be close to Rap74) or whether the proximity is enhanced by electrostatic complementarity, we next repeated the intermolecular PRE measurements using the charge-inversion mutants of ctFcp1.

Intermolecular PRE with ctFcp1 Charge Variants to Assess Their Impact on Association with Charged Regions of the Rap74 Surface. If electrostatic associations drive the interaction between acidic regions of ctFcp1's disordered tail and the basic patches on Rap74, the charge variants of ctFcp1 in which we have replaced clusters of Glu and Asp residues with Lys and Arg should display less intermolecular PRE, and vice versa for the EDE variant in which negative charge near residue 927 is reinforced. We chose to retain cystine introduction and spin-labeling at residue 927 for consistency with the intramolecular PRE data sets (Figures 2 and 3) and because this position had shown good sensitivity for intermolecular PRE from wild-type ctFcp1 to Rap74 (Figure 4). The results of the intermolecular PRE with ctFcp1 charge variants are depicted in Figure 5 (spectra in Figure S7; raw data in Table S3). We expected the EDE construct, which increased the negative charge density in the vicinity of the spin-label, to produce increased PRE on Rap74 on the positively charged face. The resulting PRE experiment does show that to be the case, but unexpectedly, we also saw decreased PRE on the face of Rap74 with neutral charge. For intermolecular PRE involving the 3K construct, which replaced acidic residues immediately surrounding the spin-label with basic ones, we correspondingly saw a near complete elimination of PRE-associated intensity loss on the surface of Rap74. The 5KR and KRK constructs, which had increased positive charge compared to wild type, also exhibited much less intermolecular PRE, although missing resonances in both spectra obscured the analysis compared to the other constructs. Taken together, these results confirm the presence of charge-mediated association between ctFcp1's disordered region and the face of Rap74 opposite to the Fcp1 binding cleft.

Equilibrium Binding Assays to Assess the Relative Strength of Binding between Rap74 and the Panel of ctFcp1 Charge Variants. Having established that there likely are electrostatically mediated interactions between the helix-flanking region of ctFcp1 and the surface of Rap74, we next set out to quantify the impact of these interactions on the strength of binding. If the intermolecular association between the two oppositely charged regions of ctFcp1 and Rap74 contributes favorably to binding, then flipping residues from acidic to basic outside the helix/cleft binding region should decrease the stability of the ctFcp1−Rap74 complex.

To evaluate the dissociation constants for binding of the various charge mutants to Rap74, we measured fluorescence anisotropy of f-Fcp1x in competitive binding assays. We chose a competition format because it allows, with proper curve fitting, for determination of the observed equilibrium constant (K_D) for the intrinsically disordered ctFcp1 and charge variants in the absence of a conjugated fluorophore, which may have perturbed the structural ensemble of ctFcp1. Direct binding assays between f-Fcp1x and Rap74 confirmed a significant change in fluorescence anisotropy upon binding (Figure 6A) and established the dissociation constant for f-Fcp1x and Rap74 as $K_d = 2.2 \pm 0.1$ μM, which is needed for proper fitting of the competitor binding constant (see the Methods section). This value is consistent with previously established dissociation constants for this system, while accounting for some variation due to different experimental buffers. In subsequent competitive binding assays, the concentration of wild-type or one of four ctFcp1 charge variants, hereafter termed "competitor", were varied across the titration while f-Fcp1x and Rap74 concentrations were held constant. The concentration of Rap74 was selected to produce an observed fluorescence anisotropy that is significantly higher than the free-ligand baseline, yet low enough to observe competition with an achievable concentration range of the competitor ligand. Upon titration, a decrease in anisotropy from f-Fcp1x was observed (Figure 6B), consistent with the fluorescently labeled probe being displaced by the (unmodified) competitor.

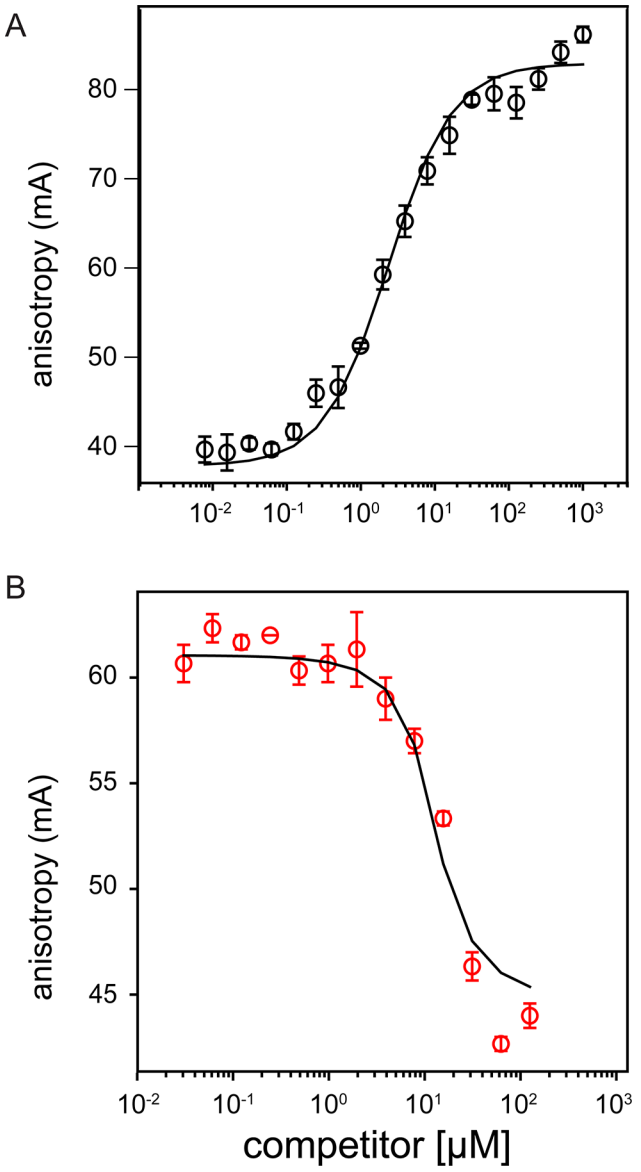

Figure 6. Competitive binding assays of Rap74 and ctFcp1 charge variants monitored by fluorescence anisotropy. (a) Representative direct titration of Rap74 against constant concentration of f-Fcp1x (a peptide containing Fcp1 residues 940−961 and an N-terminal fluorophore). Anisotropy units are arbitrary and produced by the fluorometer. (b) Representative competitor titration of wild-type ctFcp1 against Rap74 and f-Fcp1x held constant at 10 μM and 40 nm, respectively. All experiments were performed in triplicate, with error bars representing one standard deviation from the mean. Solid curves are fits to the data as described in the Methods section.

https://doi.org/10.1021/acs.jpcb.1c05131
J. Phys. Chem. B 2021, 125, 10917−10927

The observed pattern of dissociation constants for each of the charge variants revealed that modifying the charge pattern in the disordered flanking region does affect binding affinity and that the trend is consistent with a role for electrostatic complementarity in stabilizing the interaction (Table 2; titration curves in Figure S8). The K_d for the EDE construct, 0.6 ± 0.07 μM, is slightly less than the wild-type construct, 1.0 ± 0.2 μM. The K_d's for the 3K and KRK constructs were clearly higher, at 1.96 ± 0.07 and 4.0 ± 0.4 μM, respectively. Quantitative evaluation of the 5KR binding constant was not possible; we observed a sharp increase in fluorescence anisotropy at the high competitor concentrations required to saturate binding for this weakest binding construct (Figure S8E). This result is consistent with our prior observation that ctFcp1 oligomerizes at high concentration [Lawrence, C. W.; Showalter, S. A., personal communication] and with f-Fcp1x also being incorporated into oligomers with ctFcp1 5KR as its concentration increases. Overall, the ctFcp1 charge mutants with the greatest amount of negative charge in the disordered tail proved to be the tightest binders to Rap74, and as positive charge began to increase, the dissociation constant grew weaker until it was unable to be measured by fluorescence anisotropy competitive binding assays.

Table 2. Best Fit Macroscopic Binding Affinities (K_d, μM) as Determined by Fluorescence Anisotropy Competitive Binding Assays for ctFcp1 Constructs

ctFcp1 construct	dissociation constant (μM)
EDE	0.6 ± 0.07
wild type	1.0 ± 0.2
3K	1.96 ± 0.07
KRK	4.0 ± 0.4
5KR	n.d.[a]

[a]Binding unable to be determined; construct binds too weakly to Rap74 for competition assays.

DISCUSSION

In this work, we identified biases in the conformational ensemble of a model disordered protein, ctFcp1, which are driven by interactions between oppositely charged regions of the backbone. Altering charge patterning in ctFcp1 led to changes in observed PRE consistent with the detected electrostatically mediated interactions. We discovered a similar electrostatic interaction occurring intermolecularly as well, in the binding complex of ctFcp1 and Rap74. Negatively charged regions of ctFcp1 have increased association with a positively charged patch on the opposite side of Rap74, when compared to the rest of Rap74's surface. The intermolecular association appears to also be under electrostatic control, as detected via further variations in charge. We also showed the intermolecular interaction stabilizes the binding complex, as inverting the charge of positively charged and negatively charged residues in ctFcp1's disordered flanking region strengthens and weakens the binding interaction, respectively.

Because IDPs are frequently polyampholytic, we suspect interactions similar to the one characterized here exist in other IDP systems. Disordered regions adjacent to binding motifs could either stabilize or disrupt binding of IDP-folded protein complexes depending on the charge complementarity. Post-translational modifications such as acetylation or phosphorylation can alter the charge distribution of proteins further, which then could possibly impact binding stability. Lysine acetylation has been shown to lead to reduction of the net charge on the H4 histone tail.[38] Phosphorylation directly installs a negative charge onto a side-chain. In the ctFcp1/Rap74 system, phosphorylation of Ser942 and Ser944 is known to improve the stability of the bound complex, either by forming ion pairs with nearby lysines on Rap74 or through nonspecific electrostatic interactions.[39]

For our experiments involving inversion of charge in ctFcp1 disordered regions, we hypothesized binding complex stability would be more favorable in constructs where basic residues were replaced with acidic residues, and the opposite would be true for replacing acidic with basic residues. However, in the latter case, the presence of a larger positive surface for intramolecular charge-mediated interactions may increase self-occlusion of the binding helix. Charge mutants that self-occlude the binding motif would have a corresponding increase in dissociation constant compared to the wild-type sequence. It is difficult to isolate independently the impacts of self-occlusion and nonspecific interactions on binding stability and determine if one or the other dominates the interaction, underscoring the complexity of interactions facilitated by the presence of disorder in proteins.

For the Fcp1/Rap74 system, we have long suspected that oppositely charged regions of ctFcp1 nonspecifically interact in isolation and contributing to association with Rap74. Detailing these interactions has previously eluded us due to their transient, low-population nature, but here we demonstrate the utility of PRE to detect them. Thus, other studies of IDP-folded protein complexes may benefit from similar analysis. At a minimum, when possible, it is best to avoid using constructs that exclude disordered domains adjacent to binding motifs as it is becoming clear that they influence protein−protein interactions in "fuzzy" complexes.[22] No doubt, stabilizing interactions from flanking charged regions exist in other IDP/folded protein systems. Future studies, particularly those that leverage PRE, are necessary to determine whether the effect observed in the ctFcp1/Rap74 system is unique or a recurrent phenomenon in IDP interactions.

ASSOCIATED CONTENT

Supporting Information

The Supporting Information is available free of charge at https://pubs.acs.org/doi/10.1021/acs.jpcb.1c05131.

Figures S1−S8 representing raw data from all experiments; Tables S1−S3 providing numerical values of all PRE ratios (PDF)

AUTHOR INFORMATION

Corresponding Author

Scott A. Showalter − *Department of Chemistry, The Pennsylvania State University, University Park, Pennsylvania 16802, United States; Department of Biochemistry and Molecular Biology, The Pennsylvania State University, University Park, Pennsylvania 16802, United States;* orcid.org/0000-0001-5179-032X; Email: sas76@psu.edu

Authors

Victor A. Prieto − *Department of Chemistry, The Pennsylvania State University, University Park, Pennsylvania 16802, United States*

https://doi.org/10.1021/acs.jpcb.1c05131
J. Phys. Chem. B 2021, 125, 10917−10927

Kevin E. W. Namitz − *Department of Chemistry, The Pennsylvania State University, University Park, Pennsylvania 16802, United States;* orcid.org/0000-0003-4434-1475

Complete contact information is available at: https://pubs.acs.org/10.1021/acs.jpcb.1c05131

Notes

The authors declare no competing financial interest.

■ ACKNOWLEDGMENTS

This work was supported by two US National Science Foundation grants to S.A.S. (MCB-1515974, MCB-1932730). We are grateful to Dr. Tim Miyashiro for allowing access to their Tecan fluorometer. The Biostat fermentation vessel was used with permission and training at the Huck Institutes CSL Behring Fermentation Facility.

■ REFERENCES

(1) Oates, M. E.; Romero, P.; Ishida, T.; Ghalwash, M.; Mizianty, M. J.; Xue, B.; Dosztanyi, Z.; Uversky, V. N.; Obradovic, Z.; Kurgan, L.; Dunker, A. K.; Gough, J. D(2)P(2): database of disordered protein predictions. *Nucleic Acids Res.* **2012**, *41*, D508−D516.

(2) van der Lee, R.; Buljan, M.; Lang, B.; Weatheritt, R. J.; Daughdrill, G. W.; Dunker, A. K.; Fuxreiter, M.; Gough, J.; Gsponer, J.; Jones, D. T.; Kim, P. M.; Kriwacki, R. W.; Oldfield, C. J.; Pappu, R. V.; Tompa, P.; Uversky, V. N.; Wright, P. E.; Babu, M. M. Classification of intrinsically disordered regions and proteins. *Chem. Rev.* **2014**, *114* (13), 6589−631.

(3) Sigler, P. B. Transcriptional activation. Acid blobs and negative noodles. *Nature* **1988**, *333* (6170), 210−212.

(4) Tomko, R. J., Jr.; Hochstrasser, M. The intrinsically disordered Sem1 protein functions as a molecular tether during proteasome lid biogenesis. *Mol. Cell* **2014**, *53* (3), 433−443.

(5) Uversky, V. N.; Gillespie, J. R.; Fink, A. L. Why are "natively unfolded" proteins unstructured under physiologic conditions? *Proteins: Struct., Funct., Genet.* **2000**, *41* (3), 415−427.

(6) Romero, P.; Obradovic, Z.; Li, X. H.; Garner, E. C.; Brown, C. J.; Dunker, A. K. Sequence complexity of disordered protein. *Proteins: Struct., Funct., Genet.* **2001**, *42* (1), 38−48.

(7) Radhakrishnan, A.; Vitalis, A.; Mao, A. H.; Steffen, A. T.; Pappu, R. V. Improved atomistic Monte Carlo simulations demonstrate that poly-L-proline adopts heterogeneous ensembles of conformations of semi-rigid segments interrupted by kinks. *J. Phys. Chem. B* **2012**, *116* (23), 6862−6871.

(8) Das, R. K.; Pappu, R. V. Conformations of intrinsically disordered proteins are influenced by linear sequence distributions of oppositely charged residues. *Proc. Natl. Acad. Sci. U. S. A.* **2013**, *110* (33), 13392−13397.

(9) Das, R. K.; Mittal, A.; Pappu, R. V. How is functional specificity achieved through disordered regions of proteins? *BioEssays* **2013**, *35* (1), 17−22.

(10) Archambault, J.; Pan, G. H.; Dahmus, G. K.; Cartier, M.; Marshall, N.; Zhang, S.; Dahmus, M. E.; Greenblatt, J. FCP1, the RAP74-interacting subunit of a human protein phosphatase that dephosphorylates the carboxyl-terminal domain of RNA polymerase IIO. *J. Biol. Chem.* **1998**, *273* (42), 27593−27601.

(11) Meinhart, A.; Kamenski, T.; Hoeppner, S.; Baumli, S.; Cramer, P. A structural perspective of CTD function. *Genes Dev.* **2005**, *19* (12), 1401−1415.

(12) Abbott, K. L.; Archambault, J.; Xiao, H.; Nguyen, B. D.; Roeder, R. G.; Greenblatt, J.; Omichinski, J. G.; Legault, P. Interactions of the HIV-1 tat and RAP74 proteins with the RNA polymerase IICTD phosphatase FCP1. *Biochemistry* **2005**, *44* (8), 2716−2731.

(13) Showalter, S. A. NMR assignment of the intrinsically disordered C-terminal region of Homo sapiens FCP1 in the unbound state. *Biomol. NMR Assignments* **2009**, *3* (2), 179−181.

(14) Lawrence, C. W.; Bonny, A.; Showalter, S. A. The disordered C-terminus of the RNA polymerase II phosphatase FCP1 is partially helical in the unbound state. *Biochem. Biophys. Res. Commun.* **2011**, *410* (3), 461−5.

(15) Lawrence, C. W.; Showalter, S. A. Carbon-Detected (15)N NMR Spin Relaxation of an Intrinsically Disordered Protein: FCP1 Dynamics Unbound and in Complex with RAP74. *J. Phys. Chem. Lett.* **2012**, *3* (10), 1409−1413.

(16) Iesmantavicius, V.; Dogan, J.; Jemth, P.; Teilum, K.; Kjaergaard, M. Helical propensity in an intrinsically disordered protein accelerates ligand binding. *Angew. Chem., Int. Ed.* **2014**, *53* (6), 1548−1551.

(17) Rogers, J. M.; Wong, C. T.; Clarke, J. Coupled folding and binding of the disordered protein PUMA does not require particular residual structure. *J. Am. Chem. Soc.* **2014**, *136* (14), 5197−200.

(18) Kamada, K.; Roeder, R. G.; Burley, S. K. Molecular mechanism of recruitment of TFIIF-associating RNA polymerase C-terminal domain phosphatase (FCP1) by transcription factor IIF. *Proc. Natl. Acad. Sci. U. S. A.* **2003**, *100* (5), 2296−2299.

(19) Nguyen, B. D.; Abbott, K. L.; Potempa, K.; Kobor, M. S.; Archambault, J.; Greenblatt, J.; Legault, P.; Omichinski, J. G. NMR structure of a complex containing the TFIIF subunit RAP74 and the RNA polymerase II carboxyl-terminal domain phosphatase FCP1. *Proc. Natl. Acad. Sci. U. S. A.* **2003**, *100* (10), 5688−5693.

(20) Byeon, I. J.; Meng, X.; Jung, J.; Zhao, G.; Yang, R.; Ahn, J.; Shi, J.; Concel, J.; Aiken, C.; Zhang, P.; Gronenborn, A. M. Structural convergence between Cryo-EM and NMR reveals intersubunit interactions critical for HIV-1 capsid function. *Cell* **2009**, *139* (4), 780−790.

(21) Liu, Z.; Gong, Z.; Dong, X.; Tang, C. Transient protein-protein interactions visualized by solution NMR. *Biochim. Biophys. Acta, Proteins Proteomics* **2016**, *1864* (1), 115−122.

(22) Tompa, P.; Fuxreiter, M. Fuzzy complexes: polymorphism and structural disorder in protein-protein interactions. *Trends Biochem. Sci.* **2008**, *33* (1), 2−8.

(23) Sickmeier, M.; Hamilton, J. A.; LeGall, T.; Vacic, V.; Cortese, M. S.; Tantos, A.; Szabo, B.; Tompa, P.; Chen, J.; Uversky, V. N.; Obradovic, Z.; Dunker, A. K. DisProt: the Database of Disordered Proteins. *Nucleic Acids Res.* **2007**, *35*, D786−D793.

(24) Gibbs, E. B.; Cook, E. C.; Showalter, S. A. Application of NMR to studies of intrinsically disordered proteins. *Arch. Biochem. Biophys.* **2017**, *628*, 57−70.

(25) Gibbs, E. B.; Showalter, S. A. Quantitative biophysical characterization of intrinsically disordered proteins. *Biochemistry* **2015**, *54* (6), 1314−1326.

(26) Vise, P.; Baral, B.; Stancik, A.; Lowry, D. F.; Daughdrill, G. W. Identifying long-range structure in the intrinsically unstructured transactivation domain of p53. *Proteins: Struct., Funct., Genet.* **2007**, *67* (3), 526−530.

(27) Wu, K. P.; Baum, J. Detection of transient interchain interactions in the intrinsically disordered protein alpha-synuclein by NMR paramagnetic relaxation enhancement. *J. Am. Chem. Soc.* **2010**, *132* (16), 5546−5547.

(28) Cook, E. C.; Sahu, D.; Bastidas, M.; Showalter, S. A. Solution Ensemble of the C-Terminal Domain from the Transcription Factor Pdx1 Resembles an Excluded Volume Polymer. *J. Phys. Chem. B* **2019**, *123* (1), 106−116.

(29) Roehrl, M. H.; Wang, J. Y.; Wagner, G. A general framework for development and data analysis of competitive high-throughput screens for small-molecule inhibitors of protein-protein interactions by fluorescence polarization. *Biochemistry* **2004**, *43* (51), 16056−16066.

(30) Tria, G.; Mertens, H. D.; Kachala, M.; Svergun, D. I. Advanced ensemble modelling of flexible macromolecules using X-ray solution scattering. *IUCrJ* **2015**, *2*, 207−217.

(31) Bernado, P.; Mylonas, E.; Petoukhov, M. V.; Blackledge, M.; Svergun, D. I. Structural characterization of flexible proteins using small-angle X-ray scattering. *J. Am. Chem. Soc.* **2007**, *129* (17), 5656−5664.

(32) Battiste, J. L.; Wagner, G. Utilization of site-directed spin labeling and high-resolution heteronuclear nuclear magnetic resonance for global fold determination of large proteins with limited nuclear overhauser effect data. *Biochemistry* **2000**, *39* (18), 5355−5365.
(33) Pettersen, E. F.; Goddard, T. D.; Huang, C. C.; Couch, G. S.; Greenblatt, D. M.; Meng, E. C.; Ferrin, T. E. UCSF Chimera–a visualization system for exploratory research and analysis. *J. Comput. Chem.* **2004**, *25* (13), 1605−1612.
(34) Worrall, E. G.; Wawrzynow, B.; Worrall, L.; Walkinshaw, M.; Ball, K. L.; Hupp, T. R. Regulation of the E3 ubiquitin ligase activity of MDM2 by an N-terminal pseudo-substrate motif. *J. Chem. Biol.* **2009**, *2* (3), 113−129.
(35) Showalter, S. A.; Bruschweiler-Li, L.; Johnson, E.; Zhang, F.; Bruschweiler, R. Quantitative lid dynamics of MDM2 reveals differential ligand binding modes of the p53-binding cleft. *J. Am. Chem. Soc.* **2008**, *130* (20), 6472−6478.
(36) Uhrinova, S.; Uhrin, D.; Powers, H.; Watt, K.; Zheleva, D.; Fischer, P.; McInnes, C.; Barlow, P. N. Structure of free MDM2 N-terminal domain reveals conformational adjustments that accompany p53-binding. *J. Mol. Biol.* **2005**, *350* (3), 587−598.
(37) Holehouse, A. S.; Das, R. K.; Ahad, J. N.; Richardson, M. O.; Pappu, R. V. CIDER: Resources to Analyze Sequence-Ensemble Relationships of Intrinsically Disordered Proteins. *Biophys. J.* **2017**, *112* (1), 16−21.
(38) Winogradoff, D.; Echeverria, I.; Potoyan, D. A.; Papoian, G. A. The Acetylation Landscape of the H4 Histone Tail: Disentangling the Interplay between the Specific and Cumulative Effects. *J. Am. Chem. Soc.* **2015**, *137* (19), 6245−6253.
(39) Abbott, K. L.; Renfrow, M. B.; Chalmers, M. J.; Nguyen, B. D.; Marshall, A. G.; Legault, P.; Omichinski, J. G. Enhanced binding of RNAP II CTD phosphatase FCP1 to RAP74 following CK2 phosphorylation. *Biochemistry* **2005**, *44* (8), 2732−2745.

https://doi.org/10.1021/acs.jpcb.1c05131
J. Phys. Chem. B 2021, 125, 10917−10927